Improved performances toward electrochemical carbon dioxide and oxygen reductions by iron-doped stannum nanoparticles

Jiangtao Zhu[a,b†], Quan Zhang[a†], Caiyun Wang[b]*, Yanhong Feng[a], Yuanyuan Zhang[c], Gaocan Qi[d]*, Lian Kang[a], Jun Luo[e], and Xijun Liu[c]*

a) MOE Key Laboratory of New Processing Technology for Nonferrous Metals and Materials, School of Resources, Environment and Materials, Guangxi University, Nanning 530004, China.

b) Guangxi Vocational & Technical Institute of Industry, Nanning 530001, China.

c) Key Laboratory of High-precision Computation and Application of Quantum Field Theory of Hebei Province, Hebei Key Lab of Optic-electronic Information and Materials, The College of Physics Science and Technology, Hebei University, Baoding, 071002, China.

d) School of Materials Science and Engineering, Tianjin University of Technology, Tianjin 300384, China.

e) ShenSi Lab, Shenzhen Institute for Advanced Study, University of Electronic Science and Technology of China, Longhua District, Shenzhen 518110, China.

† These authors contributed equally to this work.

Authors to whom correspondence should be addressed: wangcaiyun@gxgy.edu.cn; gaocanqi@tjut.edu.cn; xjliu@gxu.edu.cn.

Experimental Section

Chemicals and materials

Fe(NO$_3$)$_3$·9H$_2$O (anhydrous, 99%), Zinc acetate (97.5%), 2-Methylimidazoleand (98.5%), SnCl$_2$ (anhydrous, 99%) are purchased from Sinopharm Chemical Reagent Co., Ltd. Methyanol (99.5%) and Ethanol (99.7%) are purchased from Sinopharm Chemical Reagent Co., Ltd.

Synthesis of Fe-Sn/NC:

The precise procedure is as follows: By using ultrasound, 900 mg of Zinc acetate and 22 mg Tin chloride have been dispersed in 10 mL of deionized water (A liquor). It took 10 mL of distilled water to completely disintegrate 2.75g of 2-methylimidazole (B liquor). A and B were mixed evenly and ultra sounded for 30 min. 15 mg Ferric nitrate are added into this liquor and agitated for 6 h at room temperature. The suspension is centrifuged to obtain a solid powder. After drying in a vacuum drying oven at 70°C for 12 h, the light-yellow brown powder obtained was named Fe-Sn/ZIF-8. Sn nanoparticles with Fe doped N-carbon framework named Fe-Sn/NC were obtained by calcining the precursor in 900°C H$_2$/Ar atmosphere for 2 h.

Synthesis of Sn/NC

Ferric nitrate is not added in the synthesis process. Other steps are the same as the synthesis of Fe-Sn/NC.

Synthesis of NC

Ferric nitrate and tin chloride are not added in the synthesis process. Other steps are the same as the synthesis of Fe-Sn/NC.

Characterization

The morphology and microstructure of the samples were characterized by field emission scanning electron microscopy (FESEM, Verios 460L). Transmission electron microscope (TEM), High angle annular dark field Scanning-Transmission Electron Microscopy (HAADF-STEM) images, and Energy Dispersive X-ray spectroscopy (EDX) mappings of the samples were characterized by using an FEI Talos F200X S with a field-emission gun at 200 kV. X-ray diffractometer (XRD) patterns were obtained by an X-ray diffractometer (Rigaku SmartLab) from 10 to 90 degrees at a scan rate of 20 min^{-1} with Cu Kα radiation (λ = 0.154598 nm). X-ray Photoelectron Spectroscopy (XPS) spectra were collected by a Thermo Scientific K-alpha XPS system (Thermo Fisher Scientific, UK) with the Al Kα radiation as the X-ray source. Inductively coupled plasma source mass spectrometer (ICP-MS, iCAP RQ, Germany). The liquid and gas products were characterized by Avance III HD 400MHz NMR and gas chromatography (Agilent GC-7890B).
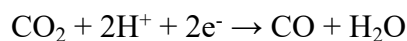
Electrochemical measurements

The electrochemical CO_2RR test was carried out in an H-type reactor separated by a Nafion 115 membrane. The electrolyte was 0.5 M $KHCO_3$ solution in compartments. Ag/AgCl electrode and Pt foil (1×1 cm^2) were used as the reference and counter electrodes, respectively. Fe-Sn/NC, Sn/NC, and NC coated on hydrophobic carbon
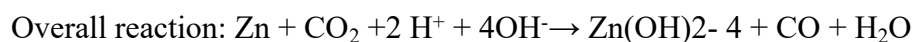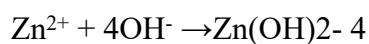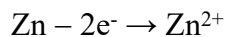
paper (1×1 cm^2) for working electrode., respectively. Firstly, 6 mg of catalyst is dispersed into 60 μL of 5 wt% Nafion solution in 0.54 mL of ethanol to prepare the catalyst ink dispersing over a period of 15-20 minute. Next, 100 μL of the catalyst ink is dropped onto carbon paper and dried it, maintaining the catalyst loading on the carbon to relative to the RHE electrode according to the following formula: $E_{RHE} = E_{Ag/AgCl} + 0.0591$ pH $+ 0.197$.

The aqueous Zn-CO_2 electrochemical was performed in H-cell, which assembles with Sn/Fe-NC (1×1 cm^{-2}) in catholyte (CO_2-saturated 0.5 M $KHCO_3$) as the cathode and 2×5 cm^{-2} Zn plate immersing in anolyte (6 M KOH + 0.2 M $Zn(CH_3COO)_2$) as the anode. The amphoteric electrolyte was separated by a bipolar membrane, which composites negative and positive membrane and causes H_2O dissociating into H^+ and OH^- under the direct current electric field. During the discharging process, 30 mL min^{-1} CO_2 continuously aerates into the catholyte causing CO product evolution ($CO_2 + 2H^+ + 2e^- \rightarrow H_2O + CO$) and Zn plate dissolution (Zn $+4OH^- \rightarrow Zn(OH)2- 4 + 2e^-$). Regarding cathodic reaction, CO_2 reduction capably occurs in near-neutral electrolytes, which prevent acidic CO_2 from reacting with an alkaline electrolyte. For anodic Zn/Zn(OH)2- 4, the near-neutral electrolyte is insufficient to driven Zn dissolution. Therefore, alkaline KOH and near-neutral $KHCO_3$ are adopted to actuate Zn/Zn(OH)2- 4 and CO_2RR, respectively. The possible charge-discharge reactions of an aqueous Zn-CO_2 battery are assumed as below:

Cathode (0.5 M $KHCO_3$ sat. CO_2)

$$CO_2 + 2H^+ + 2e^- \rightarrow CO + H_2O$$

Anode (6 M KOH with 0.2 M $Zn(CH_3COO)_2$)

$$Zn - 2e^- \rightarrow Zn^{2+}$$

$$Zn^{2+} + 4OH^- \rightarrow Zn(OH)2\text{-} 4$$

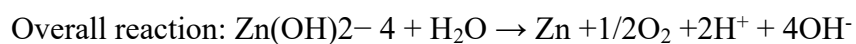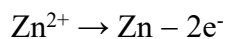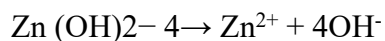Overall reaction: $Zn + CO_2 + 2 H^+ + 4OH^- \rightarrow Zn(OH)2\text{-} 4 + CO + H_2O$

During the charging process, the half-reactions on the electrode can be described as:

Cathode (0.5 M $KHCO_3$ sat. CO_2)

$$H_2O \rightarrow 1/2O_2 + 2H^+ + 2e^-$$

Anode (6 M KOH with 0.2 M $Zn(CH_3COO)_2$)

$$Zn (OH)2- 4 \rightarrow Zn^{2+} + 4OH^-$$

$$Zn^{2+} \rightarrow Zn - 2e^-$$

Overall reaction: $Zn(OH)2- 4 + H_2O \rightarrow Zn + 1/2O_2 + 2H^+ + 4OH^-$

Products analysis.

Gas chromatography (GC, Agilent GC-7890B) equipped with thermal conductivity detector (TCD) and 1H nuclear magnetic resonance (1H NMR, AVANCE AV III 400 Bruker) were used to analyze gas and liquid products, respectively. There are no significant peak signals of the liquid products display in the 1H NMR spectrum. Before gas products feeding to GC, all the outlet CO_2 flow rate was collected by an air pocket, which avoids extra water vapor causing the chromatographic column damage. The flow

rate feeding to air pocket is equal to inlet CO_2 flow rate (i.e., the total volume of outlet gas product equals to inlet CO_2 volume). Subsequently, the collected gas product was fed to GC by the air pocket for detected the average fraction of CO/H_2.

The FE_{CO}/H_2 was described as below:

$$FE_{CO/H2} \, (\%) = (2 \times m \times F)/Q = (2C_{gas} \times V_{CO2} \times 10^{-3} \times t \times F)/24.8Q$$

where m is the mol amount of CO generated; F is the Faraday constant ($96485 \, \text{C mol}^{-1}$); Q is the total quantity of electric charge during the electrolysis at a constant current density; C_{gas} is the volume concentration of the gas-phase products, calculated based on the GC results; V_{CO2} is the flow rate of CO_2 ($30 \, \text{ml min}^{-1}$); t is electrolysis time.

Figures and Table
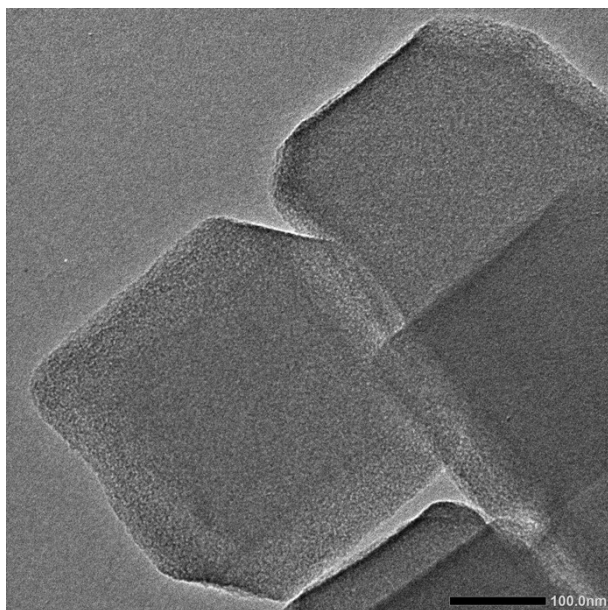
Fig. S1 SEM images of NC.
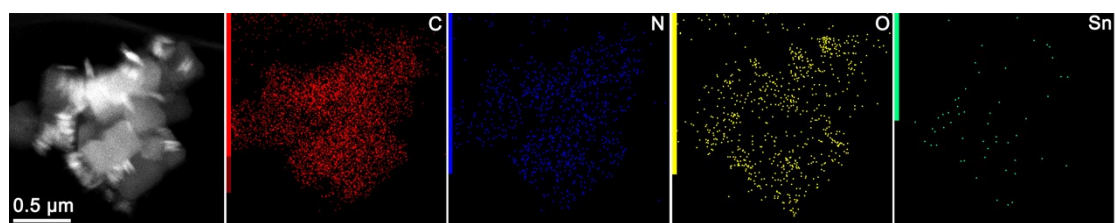
Fig. S2 EDS mapping of Sn/NC catalyst.
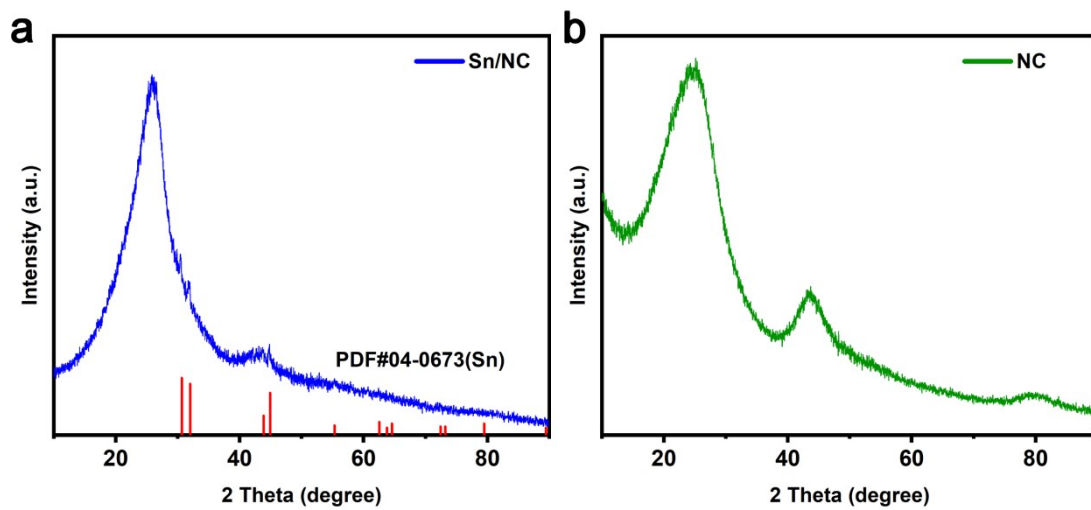
Fig. S3 The XRD patterns of NC and Sn/NC.
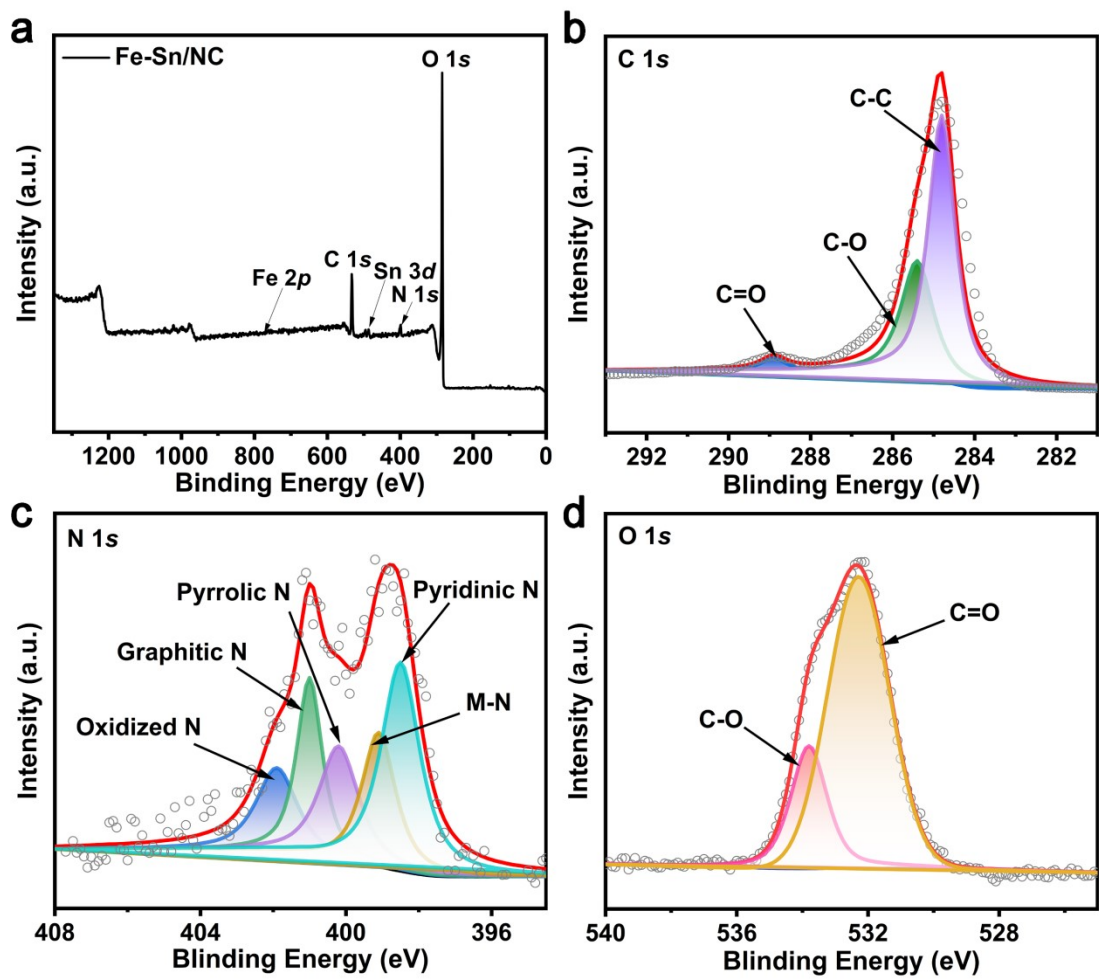
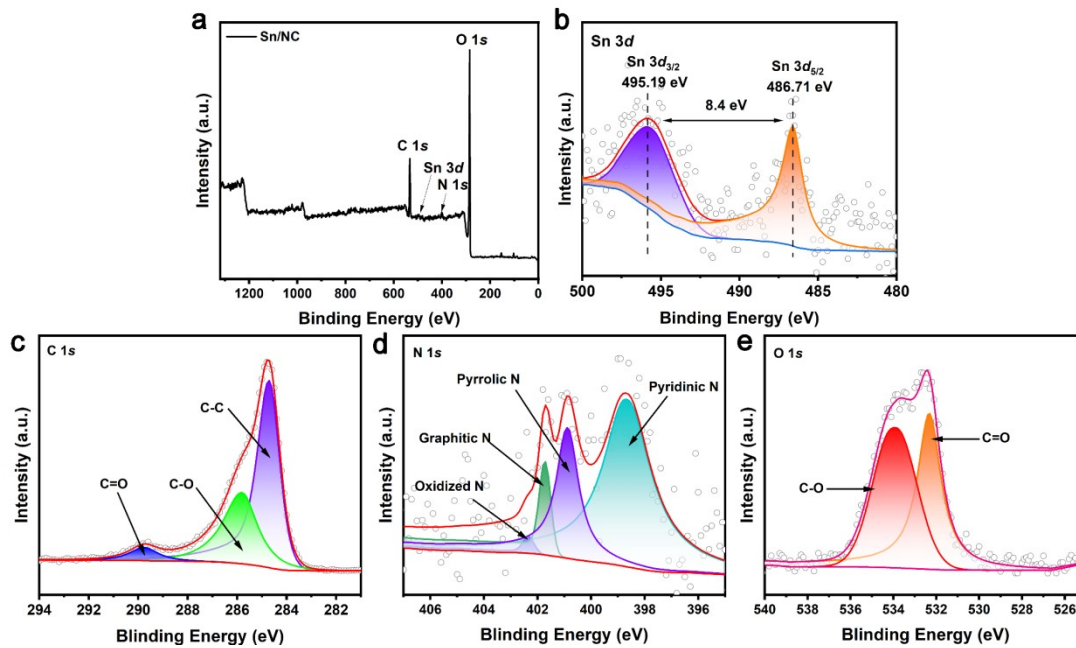**Fig. S4** XPS spectra of the full spectrum, C 1*s*, N 1*s* and O 1*s*.

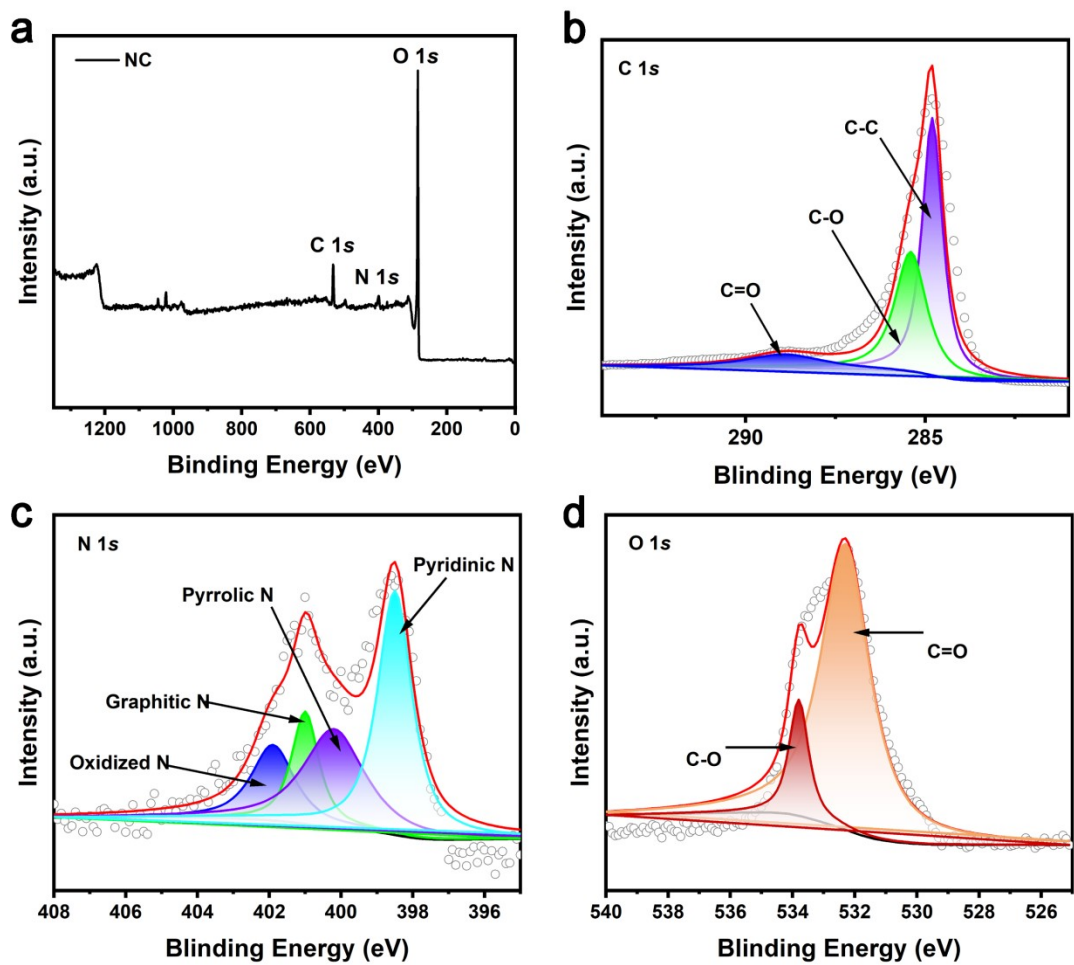**Fig. S5** XPS spectra of the full spectrum, Sn 3*d*, C 1*s*, N 1*s* and O 1*s*.

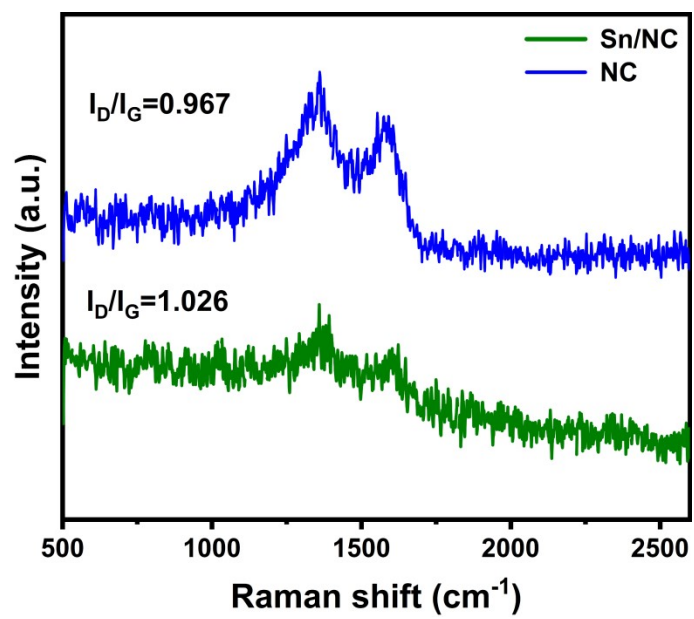**Fig. S6** XPS spectra of the full spectrum, C 1*s*, N 1*s* and O 1*s*.
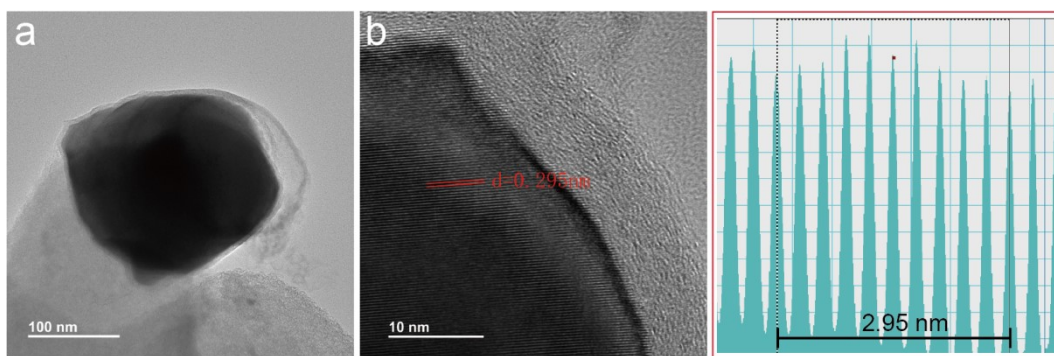
Fig. S7 Raman spectrum of Sn/NC and NC.

Fig. S8 (a) TEM images of Fe-Sn/NC catalyst; (b) High-resolution TEM images of Fe-Sn/NC catalyst.
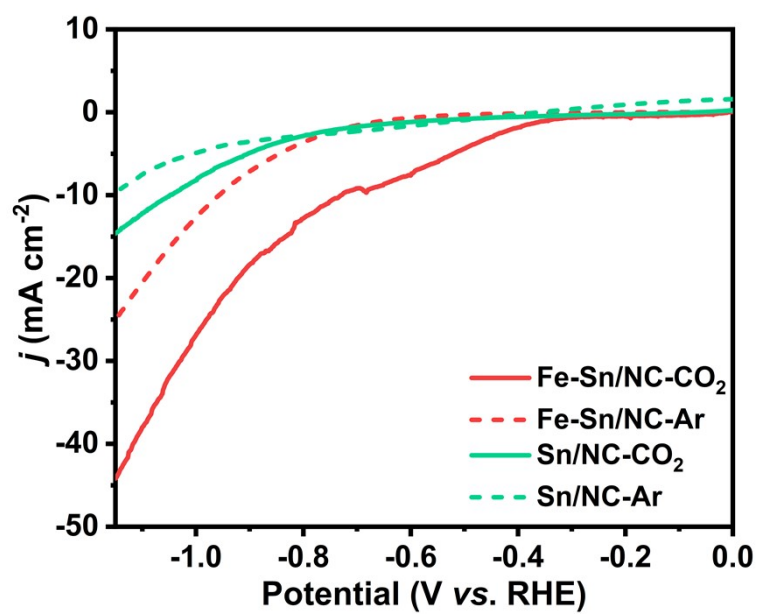
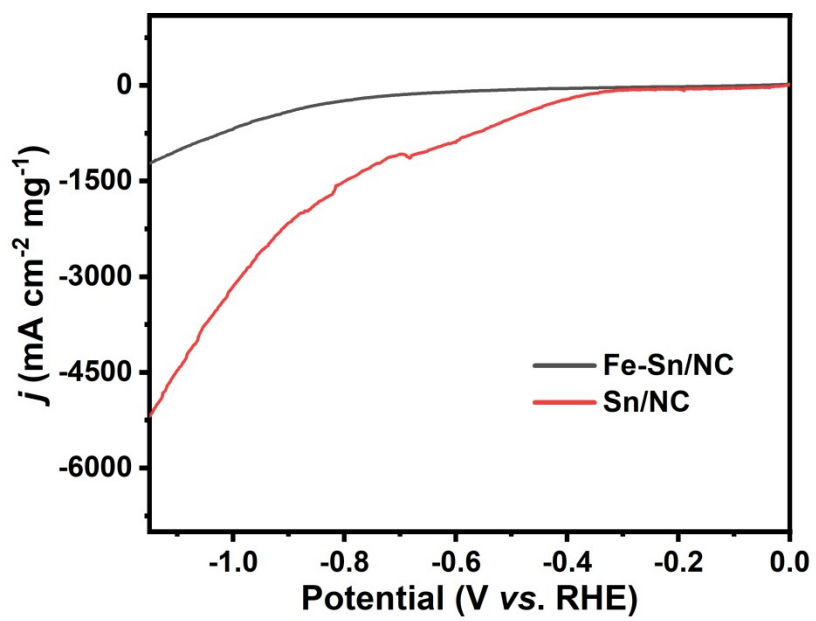**Fig. S9** LSV of Fe-Sn/NC and Sn/NC in CO_2 or Ar saturated 0.5 M $KHCO_3$.
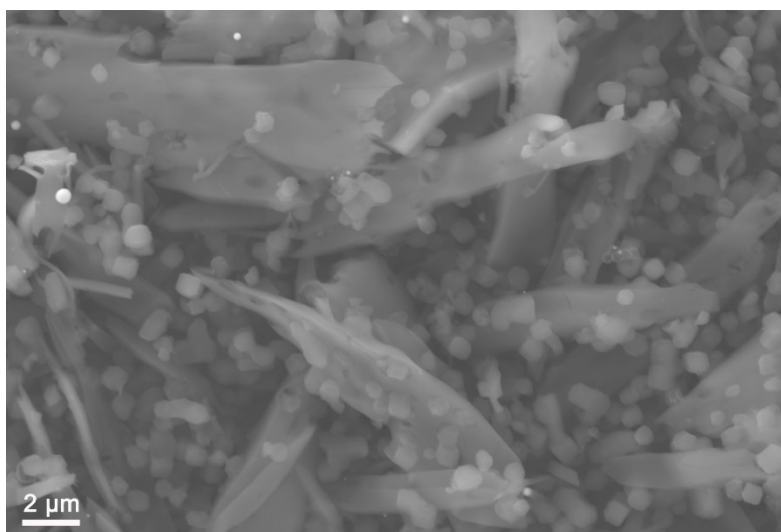
Fig. S10 LSV curve normalized by Sn mass.

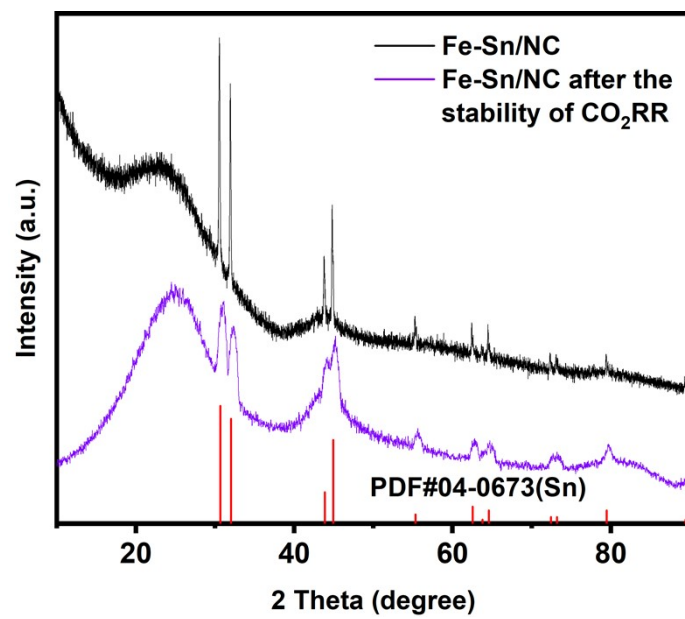**Fig. S11** SEM of Fe-Sn/NC after the stability of CO_2RR.

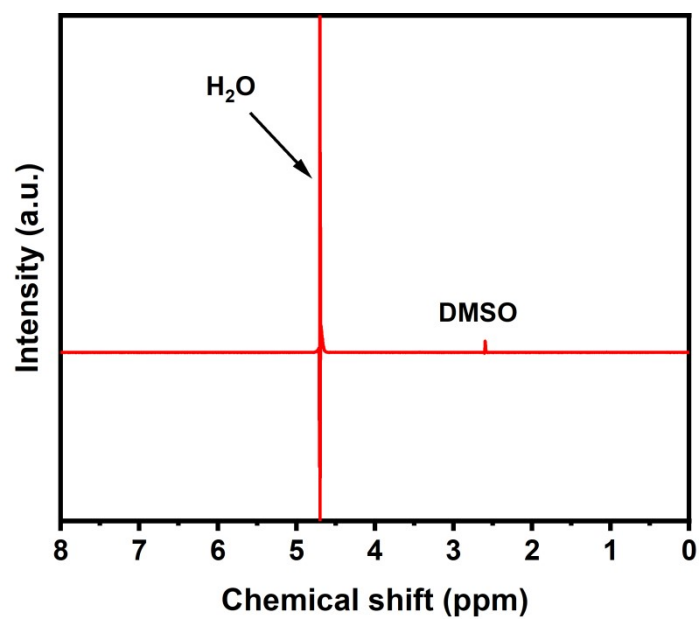**Fig. S12** The XRD patterns of Fe-Sn/NC after the stability of CO_2RR.

Fig.S13 1H NMR spectrum of the liquid product, collecting from the stability of CO_2RR, electrolyte solution was collected from the cathode chamber after electrolysis and characterized by Avance III HD 400MHz 1H nuclear magnetic resonance (1H NMR) and no liquid reduction product can be detected.
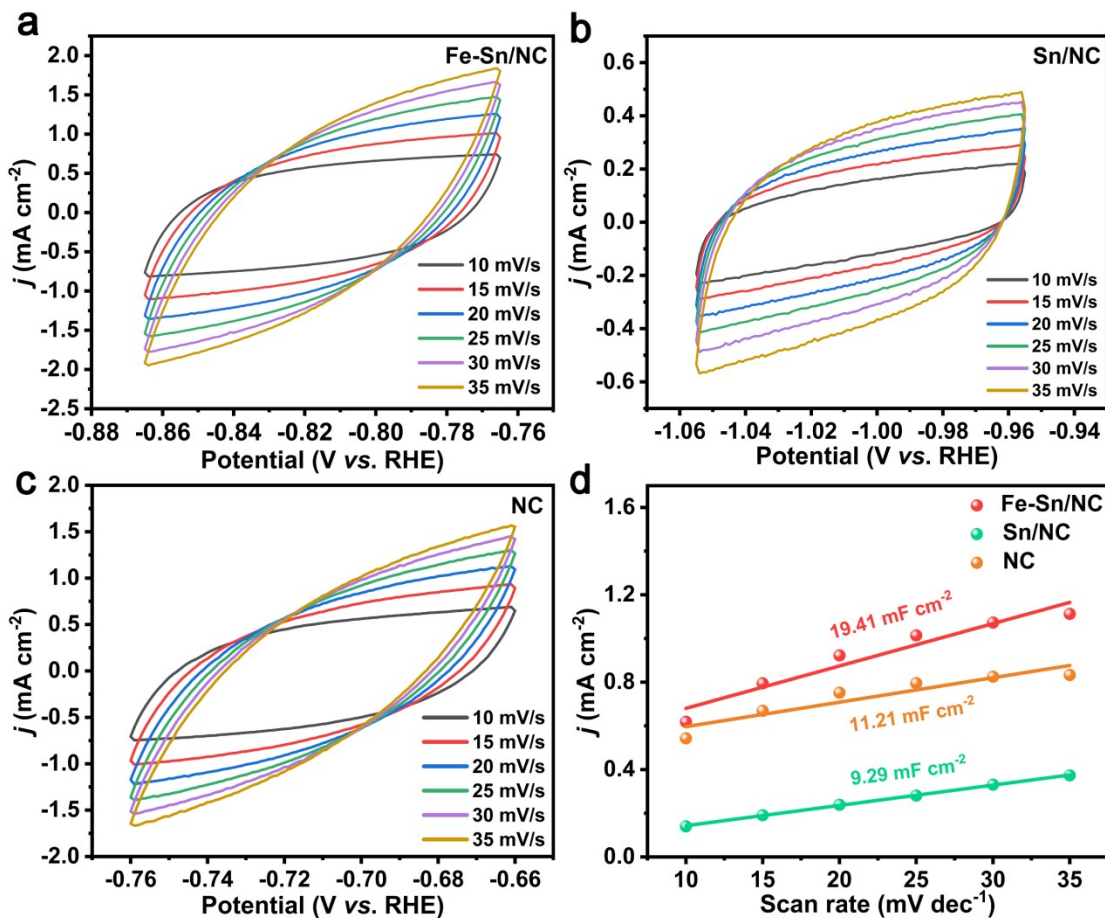
Fig. S14 (a), (b) and (c) ECSA of Fe-Sn/NC, Sn/NC and NC in CO_2RR; (d) C_{dl} of Fe-Sn/NC, Sn/NC and NC.

$j_{ECSA} = j*40 \ \mu F/C_{dl}$

From the above formula, the ECSA of the Fe-Sn/NC, Sn/NC, and NC[1,2]:

A_{ECSA} Fe-Sn/NC = 19410μF/40 μF cm^{-2} = 485.25 cm^2
A_{ECSA} Sn/NC = 11210 μF/40 μF cm^{-2}= 280.25 cm^2
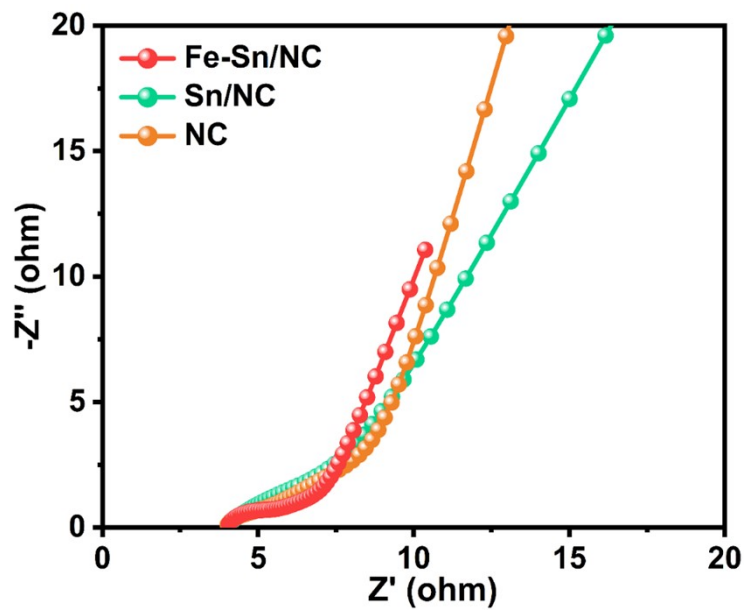A_{ECSA} NC = 9290 μF/40 μF cm^{-2} = 232.25 cm^2

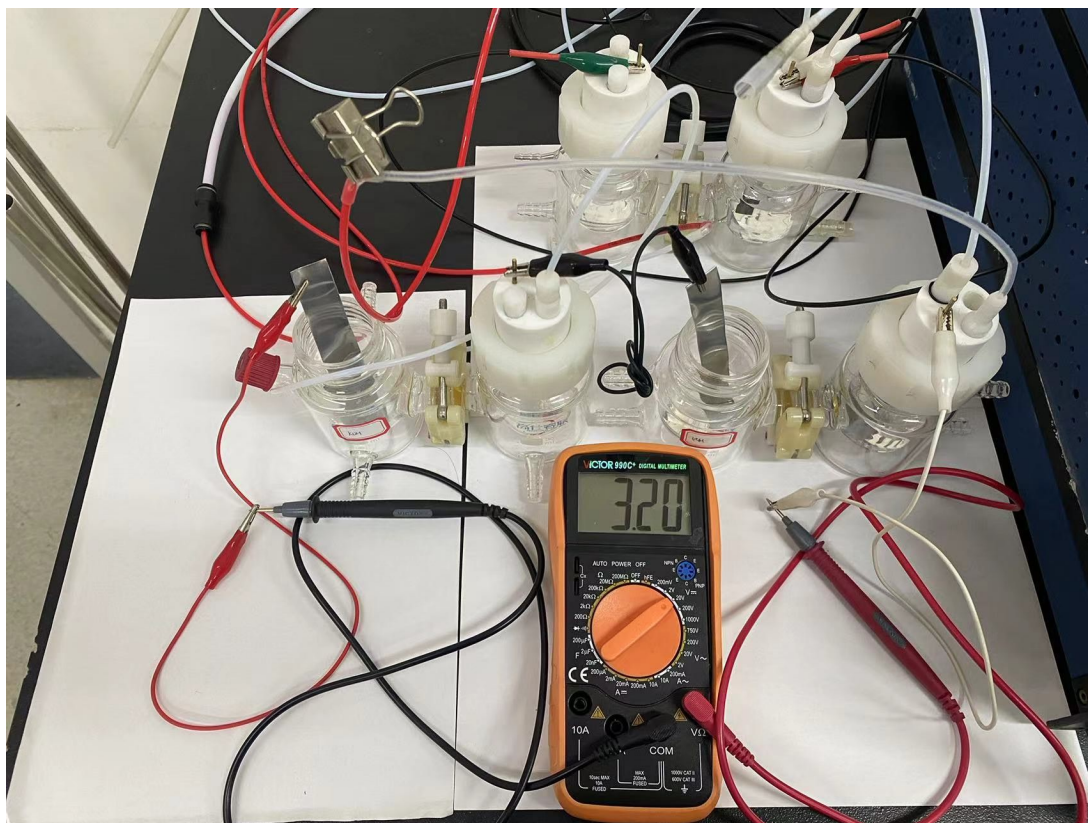**Fig. S15** EIS of Fe-Sn/NC, Sn/NC and NC.

Fig. S16 The schematic diagram of Zn–CO$_2$ battery driven CO$_2$RR.
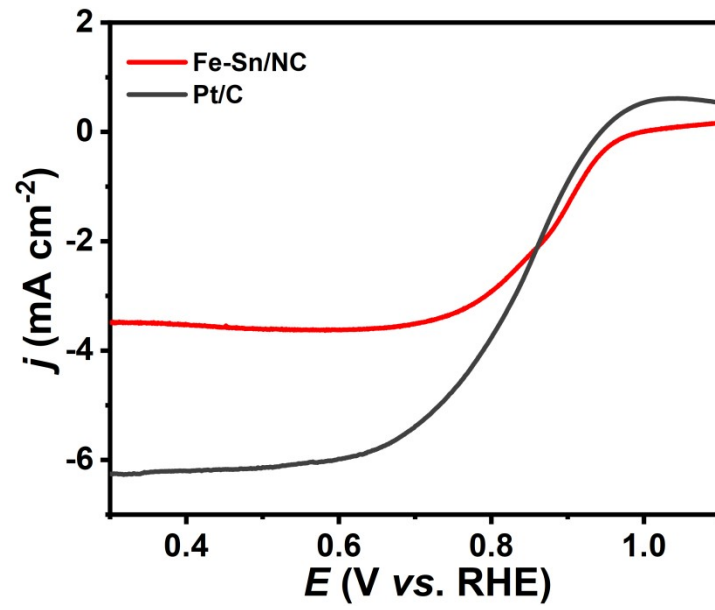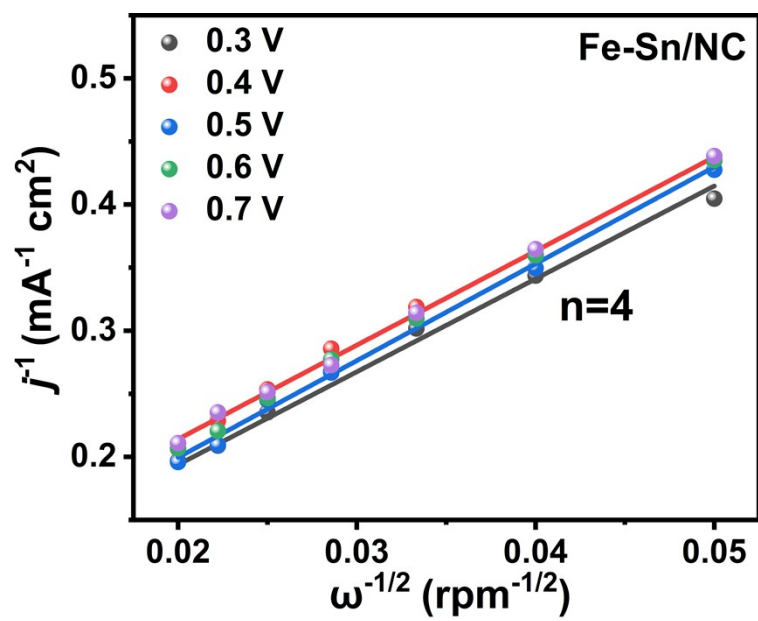
Fig. S17 LSV of Fe-Sn/NC and Pt/C in ORR.

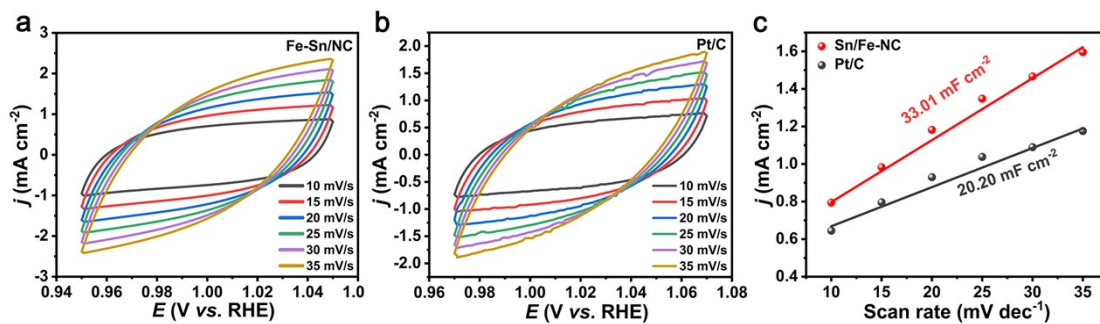**Fig. S18** The K–L plots at different potentials.

Fig. S19 (a) and (b) ECSA of Fe-Sn/NC and Pt/C in ORR, (c) C_{dl} of Fe-Sn/NC and Pt/C.

$j_{ECSA} = j*40\ \mu F/C_{dl}$

From the above formula, the ECSA of the Fe-Sn/NC and Pt/C:

A_{ECSA} Fe-Sn/NC = 33010 μF/40 μF cm^{-2} = 825.25 cm^2
A_{ECSA} Pt/C = 20200 μF/40 μF cm^{-2} = 505 cm^2
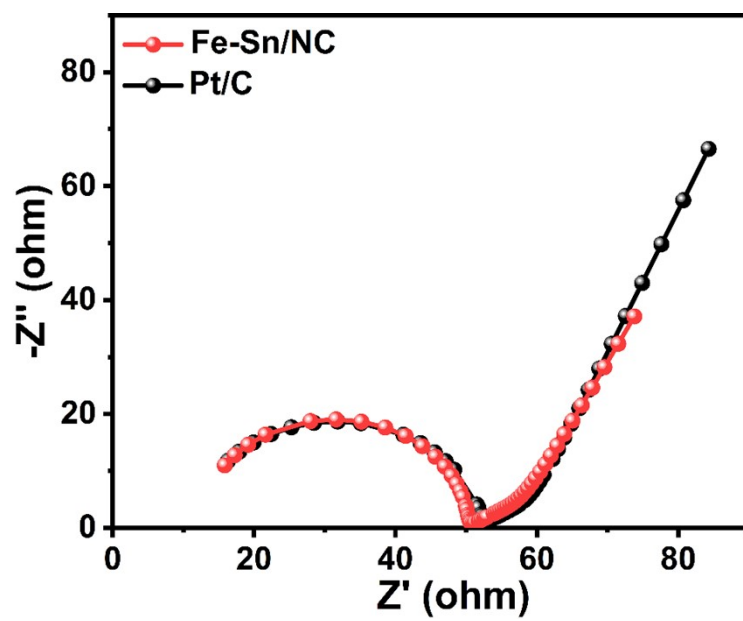
Fig. S20 EIS of Fe-Sn/NC and Pt/C in ORR.
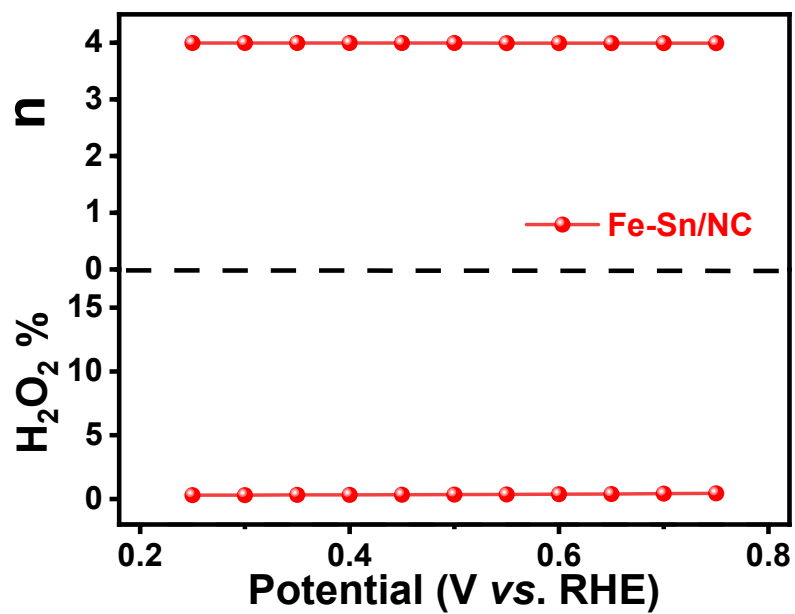
Fig. S21 The H_2O_2 yield rate and the electron transfer number n in O_2-saturated 0.1 M KOH.
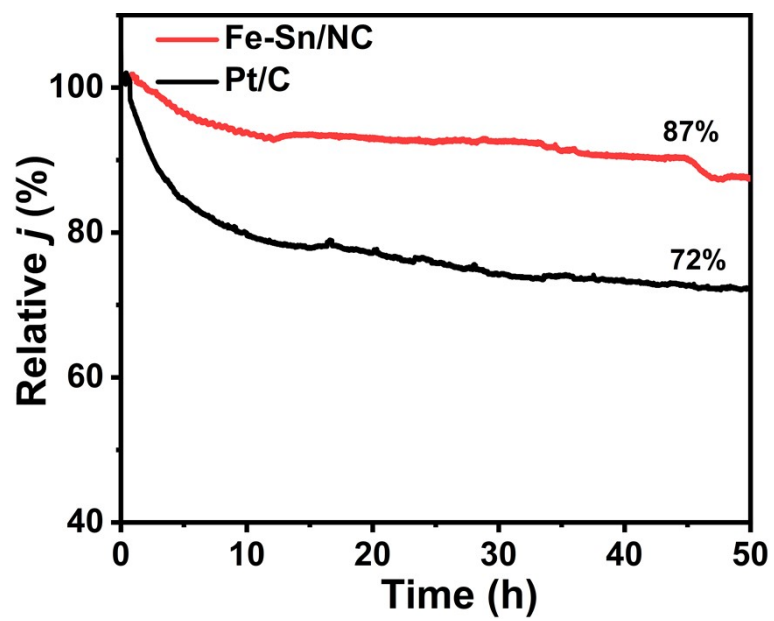
Fig. S22 The stability of the constant voltage discharge test was tested at 0.6 V.
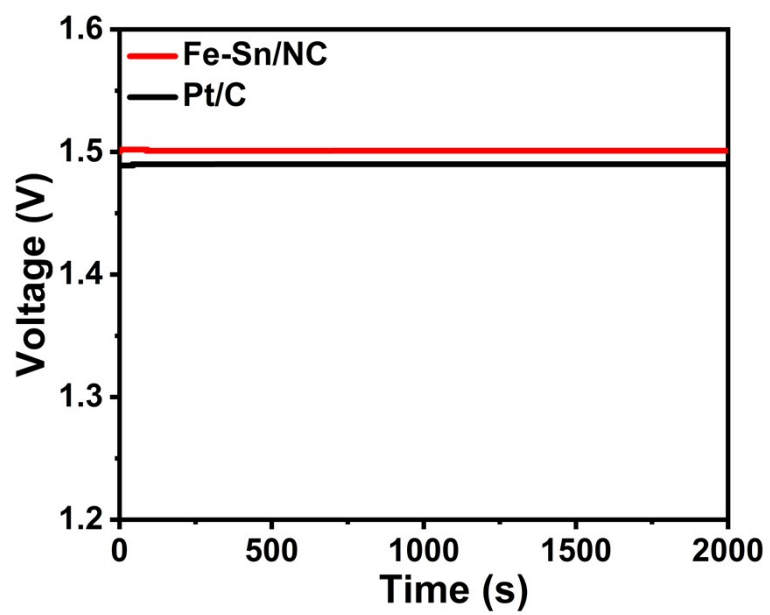
Fig. S23 The open circuit voltage of ZAB.
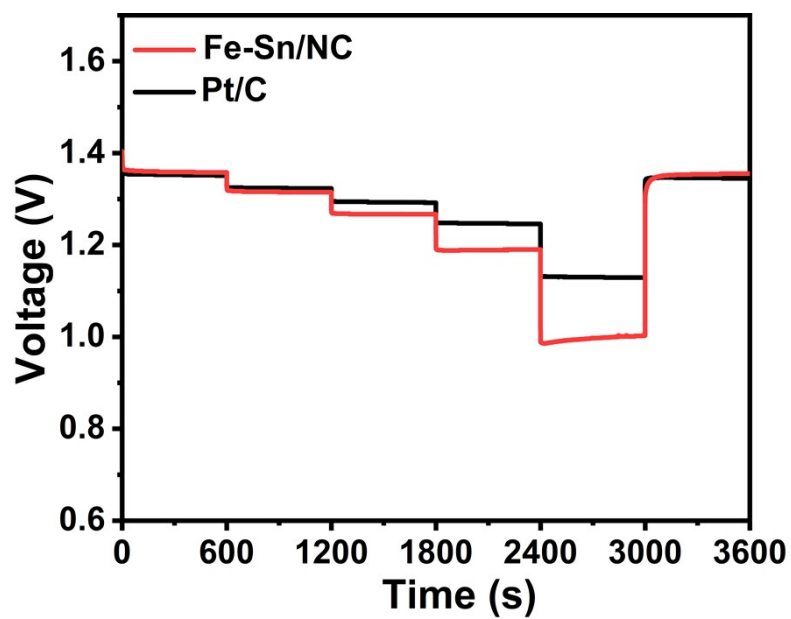
Fig. S24 The discharge steps of the ZAB assembled with Fe-Sn/NC and Pt/C.
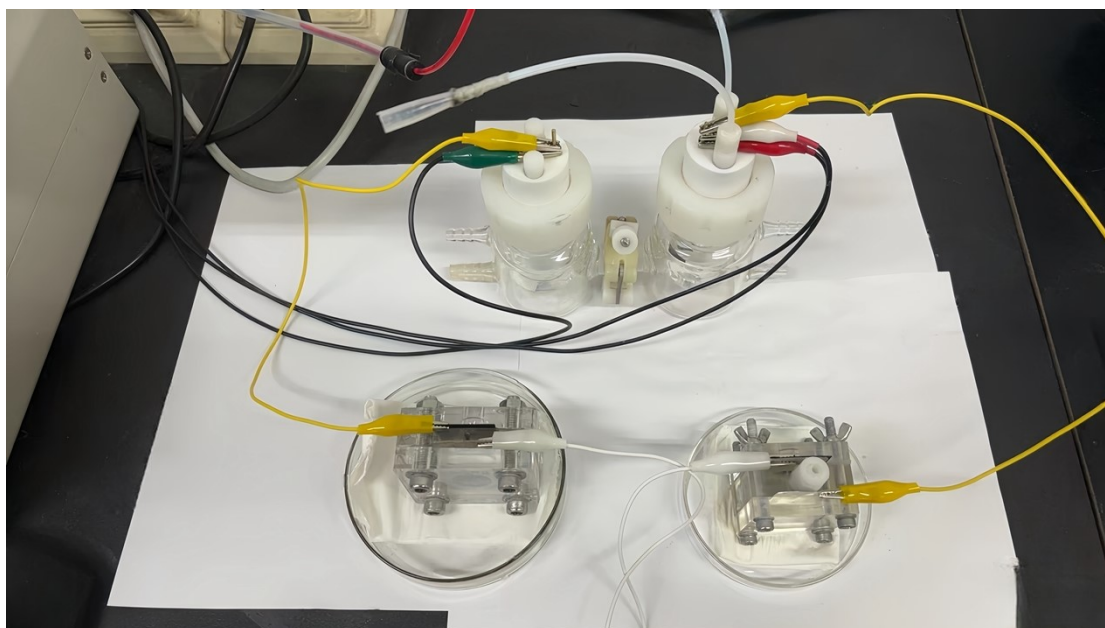
Fig. S25 The schematic diagram of Zn–Air battery driven CO$_2$RR.
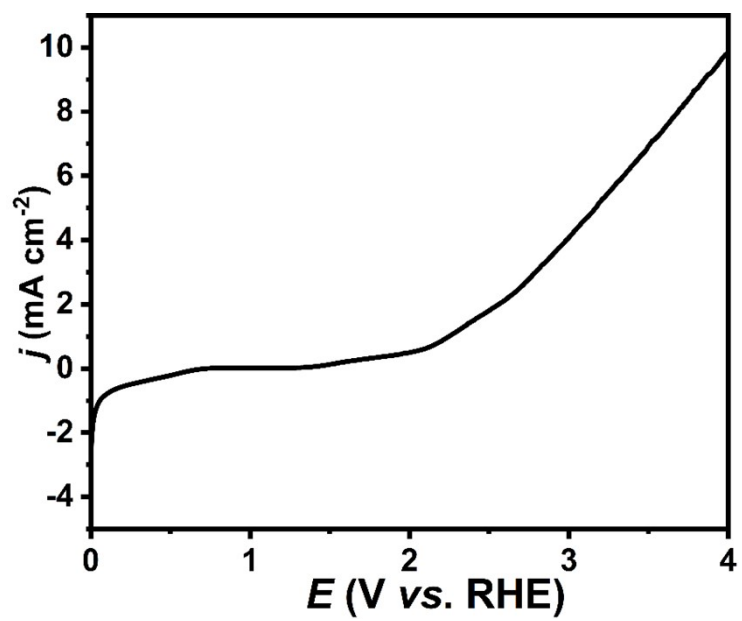
Fig. S26 LSV of Fe-Sn/NC with Zn–CO$_2$ battery driven CO$_2$RR.
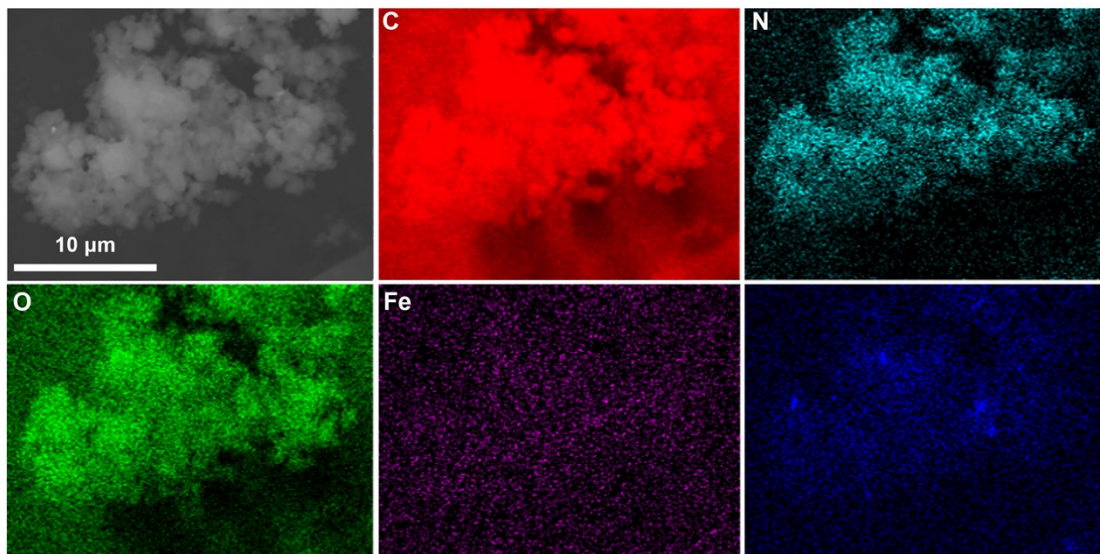
Fig. S27 SEM image and the corresponding elemental mapping of Fe-Sn/NC-10-22.
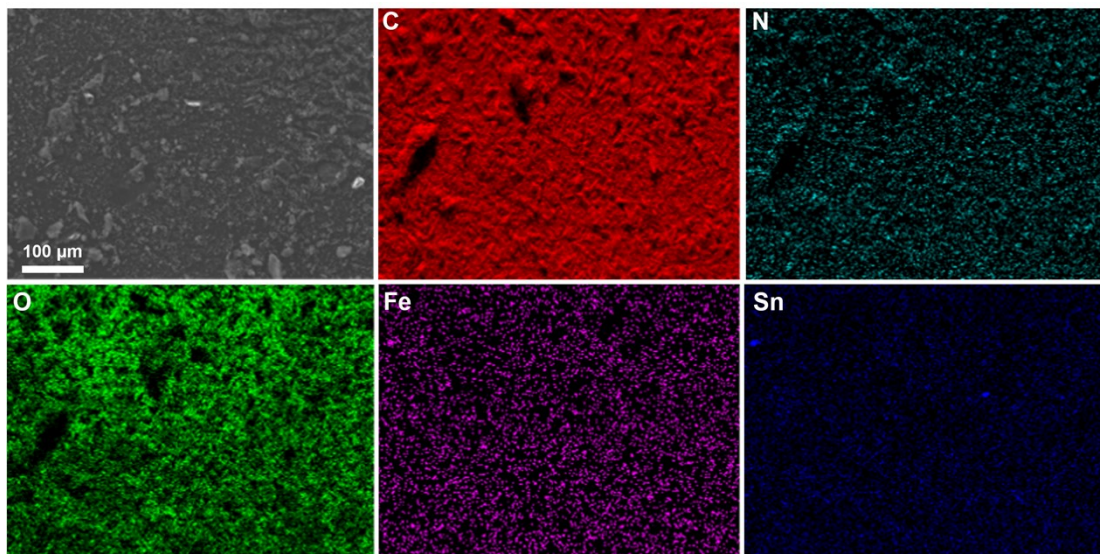
Fig. S28 SEM image and the corresponding elemental mapping of Fe-Sn/NC-15-11.
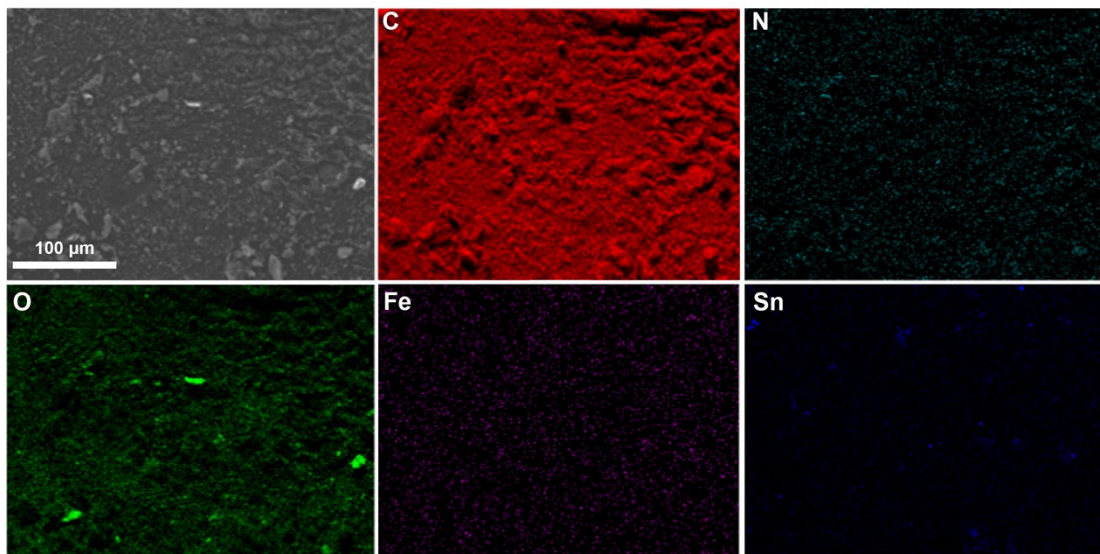
Fig. S29 SEM image and the corresponding elemental mapping of Fe-Sn/NC-15-33.
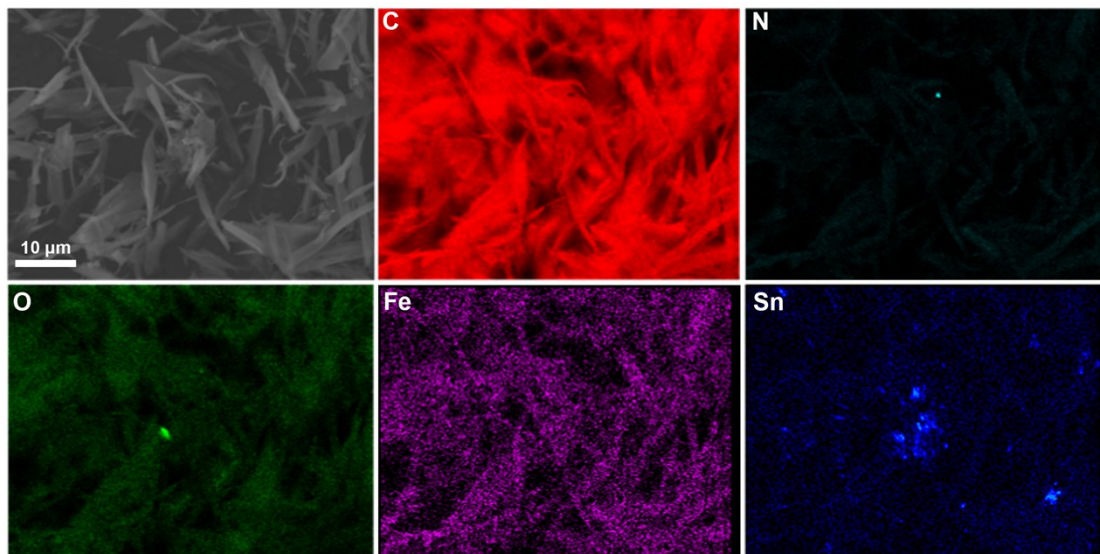
Fig. S30 SEM image and the corresponding elemental mapping of Fe-Sn/NC-20-22.
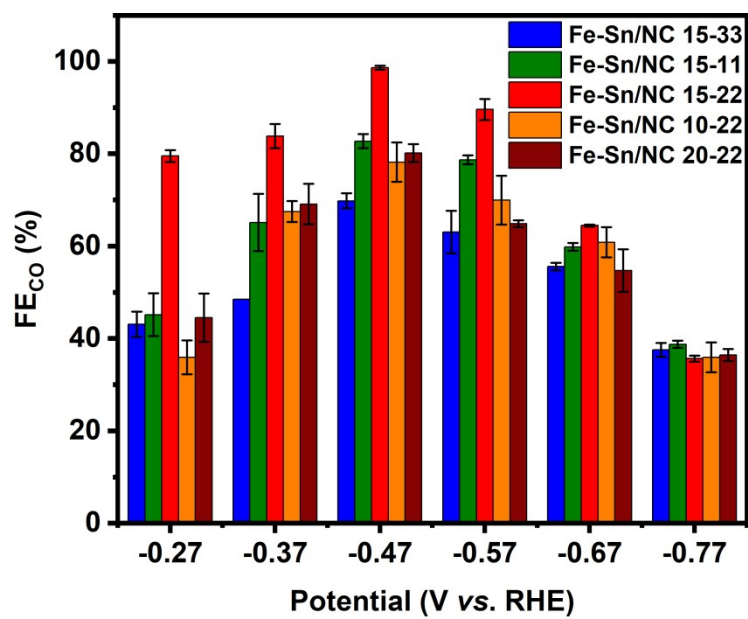
Fig. S31 The FE$_{CO}$ production at a specific potential for the samples with different ratios of Fe and Sn.
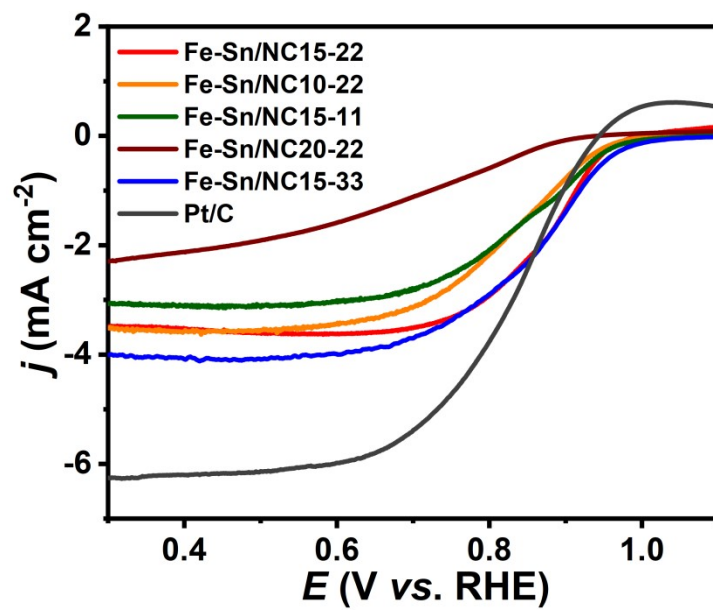
Fig. S32 The LSV curves of samples with different ratios of Fe and Sn at different rotating speeds.
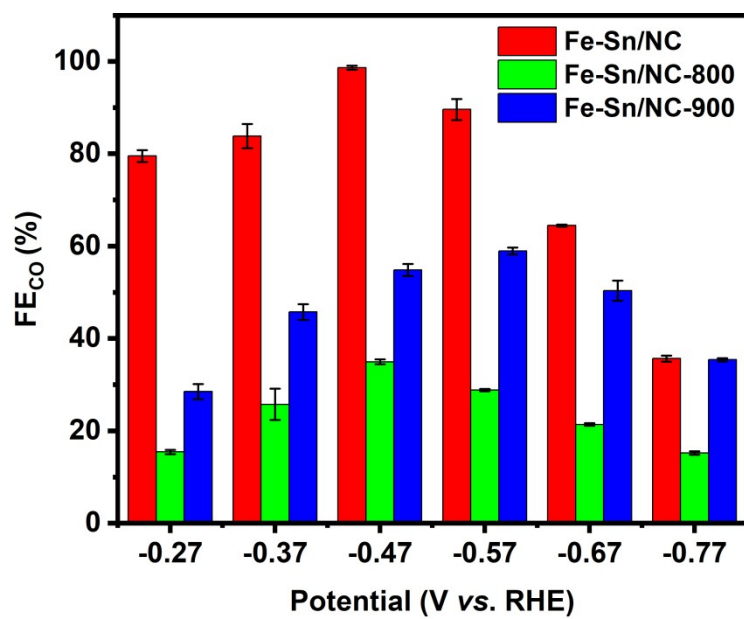
Fig. S33 The FE_{CO} generated at a specific potential for samples synthesized at different calcination temperatures.

Table S1 Fe and Sn content of Fe-Sn/NC and Sn/NC identified by ICP-MS.

Catalyst	Fe (wt.%)	Sn (wt.%)
Fe-Sn/NC	0.22	0.85
Sn/NC	0	1.19

Table S2 Fe and Sn element content analyzed by EDS

Sample	Element	At/%
Fe-Sn/NC 10-22	Fe	0.02
	Sn	0.06
Fe-Sn/NC 20-22	Fe	0.08
	Sn	0.05
Fe-Sn/NC 15-11	Fe	0.55
	Sn	0.40
Fe-Sn/NC 15-33	Fe	0.74
	Sn	1.20

Table S3 Comparison of CO_2RR performances between Fe-Sn/NC and other electrocatalysts.

Catalyst	Electrolyte	Onset potential (V)	products	FE	Stability(h)	Ref.
Fe-Sn/NC	0.5 M KHCO$_3$	-0.47	CO (g)	99%	105h	This work
Fe$_1$/PNG	0.5 M KHCO$_3$	-0.4	CO (g)	99%	50h	[3]
Fe$_2$C/Fe$_4$N@DC	0.1 M KHCO$_3$	-0.7	CO (g)	97%	24h	[4]
Fe-FN-C GDE	0.5 M KHCO$_3$	-0.5	CO (g)	93%	10h	[5]
SnPc/CNT-OH	1.0 M KHCO$_3$	-1.0	HCOOH (l)	89%	8h	[6]
Fe$_2$−N$_6$−C-o	0.5 M KHCO$_3$	-1.0	CO (g)	80%	21h	[7]
Sn$_3$O(OH)$_2$C$_{12}$	0.5 M KHCO$_3$	-0.9	HCOOH (l)	96%	40h	[8]
FeNi−NSC	0.5 M KHCO$_3$	-0.9	CO (g)	96%	12h	[9]
Vo-CuO (Sn)	0.5 M KHCO$_3$	-0.5	CO (g)	99%	180h	[10]
Fe$_2$NPC	0.1 M KHCO$_3$	-0.6	CO (g)	96%	12h	[11]
M-TTCOFs (Fe)	0.5 M KHCO$_3$	-0.7	CO(g)	91%	40h	[12]

Table S4 Summary of reported electrochemical catalysts for Zn-CO_2 battery.

Catalyst	Electrolyte	Discharge products	Power density (mW cm^{-2})	Stability(h)	Ref.
Fe-Sn/NC	0.5 M KHCO$_3$	CO (g)	1.36 mW cm^{-2}	26 h	This work
Ni–N$_4$ sites	0.5 M KHCO$_3$	CO (g)	1.4 mW cm^{-2}	20 h	[13]
Ni and Fe single atoms in N-doped graphene	2.0 M KCl	CO (g)	1.36 mW cm^{-2}	90 h	[14]
FeNC NSs-1000	0.5 M KHCO$_3$	CO (g)	1.05 mW cm^{-2}	30 h	[15]
Fe$_1$NC/S$_1$-1000	0.8 M KHCO$_3$	CO (g)	2.5 mW cm^{-2}	25 h	[16]
Cu–N$_2$/GN	0.5 M KHCO$_3$	CO (g)	1.06 mW cm^{-2}	33 h	[17]
BiPdC	0.1 M KHCO$_3$	HCOOH (l)	0.42 mW cm^{-2}	45 h	[18]
Ni–N$_3$–NCNFs	0.5 M KHCO$_3$	CO (g)	1.05 mW cm^{-2}	46 h	[19]
Zn/NC NSs	0.5 M KHCO$_3$	CO (g)	1.8 mW cm^{-2}	25 h	[20]
N-doped Carbon(NCs)	0.8 M KHCO$_3$	CO (g)	0.51 mW cm^{-2}	20 h	[21]
SAs Fe-N$_4$ @ Porous Carbon	1.0 M KHCO$_3$	CO (g)	0.925 mW cm^{-2}	50 h	[22]

References

1. Y. Gao, T. Xiong, Y. Li, Y. Huang, Y. Li and M. J. T. Balogun, *ACS Omega*, 2019, **4**, 16130-16138.
2. T. Xiong, Z. Zhu, Y. He, M. S. Balogun and Y. Huang, *Small Methods*, 2023, **7**, e2201472.
3. Q. Zhang, H. J. Tsai, F. Li, Z. Wei, Q. He, J. Ding, Y. Liu, Z. Y. Lin, X. Yang, Z. Chen, F. Hu, X. Yang, Q. Tang, H. B. Yang, S. F. Hung and Y. Zhai, *Angew. Chem. Int. Ed.*, 2023, **62**, e202311550.
4. J. Su, D. Pan, Y. Dong, Y. Zhang, Y. Tang, J. Sun, L. Zhang, Z. Tian and L. Chen, *Adv. Energy Mater.*, 2023, **13**, 2204391.
5. Y. Chen, G. Li, Y. Zeng, L. Yan, X. Wang, L. Yang, Q. Wu and Z. Hu, *Nano Res.*, 2022, **15**, 7896-7902.
6. Y. Deng, J. Zhao, S. Wang, R. Chen, J. Ding, H.-J. Tsai, W.-J. Zeng, S.-F. Hung, W. Xu, J. Wang, F. Jaouen, X. Li, Y. Huang and B. Liu, *J. Am. Chem. Soc.*, 2023, **145**, 7242-7251.
7. Y. Wang, B. J. Park, V. K. Paidi, R. Huang, Y. Lee, K.-J. Noh, K.-S. Lee and J. W. Han, *ACS Energy Letters*, 2022, **7**, 640-649.
8. T. Wang, J. D. Chen, X. Y. Ren, J. C. Zhang, J. Ding, Y. H. Liu, K. H. Lim, J. H. Wang, X. N. Li, H. B. Yang, Y. Q. Huang, S. Kawi and B. Liu, *Angew. Chem. Int. Ed.*, 2023, **62**, e202211174.
9. K. Huang, R. Li, H. Qi, S. Yang, S. An, C. Lian, Q. Xu, H. Liu and J. Hu, *Acs Catal.*, 2024, **14**, 8889-8898.
10. X. Zhong, S. Liang, T. Yang, G. Zeng, Z. Zhong, H. Deng, L. Zhang and X. Sun, *ACS Nano*, 2022, **16**, 19210-19219.
11. Y. Shi, Y. Ji, J. Long, Y. Liang, Y. Liu, Y. Yu, J. Xiao and B. Zhang, *Nat. Commun.*, 2020, **11**, 3415.
12. X. Zhao, K. Zhao, Y. Liu, Y. Su, S. Chen, H. Yu and X. Quan, *Acs Catal.*, 2022, **12**, 11412-11420.
13. W. Zheng, F. Chen, Q. Zeng, Z. Li, B. Yang, L. Lei, Q. Zhang, F. He, X. Wu and Y. Hou, *Nanomicro Lett.*, 2020, **12**, 108.
14. Z. Zeng, L. Y. Gan, H. Bin Yang, X. Su, J. Gao, W. Liu, H. Matsumoto, J. Gong, J. Zhang, W. Cai, Z. Zhang, Y. Yan, B. Liu and P. Chen, *Nat. Commun.*, 2021, **12**, 4088.
15. D. Lin, T. Wang, Z. Zhao, Y. Liu, H. Song, X. Yang, Z. Li, S. Yao, X. Hu, L. Lei, B. Yang and Y. Hou, *Nano Energy*, 2023, **113**, 108568.
16. T. Wang, X. Sang, W. Zheng, B. Yang, S. Yao, C. Lei, Z. Li, Q. He, J. Lu, L. Lei, L. Dai and Y. Hou, *Adv. Mater.*, 2020, **32**, e2002430.
17. W. Zheng, J. Yang, H. Chen, Y. Hou, Q. Wang, M. Gu, F. He, Y. Xia, Z. Xia, Z. Li, B. Yang, L. Lei, C. Yuan, Q. He, M. Qiu and X. Feng, *Adv. Funct. Mater.*, 2019, **30**, 1907658.
18. S. Gao, S. Chen, Q. Liu, S. Zhang, G. Qi, J. Luo and X. Liu, *ACS Appl. Nano Mater.*, 2022, **5**, 12387-12394.
19. W. Zheng, Y. Wang, L. Shuai, X. Wang, F. He, C. Lei, Z. Li, B. Yang, L. Lei, C. Yuan, M. Qiu, Y. Hou and X. Feng, *Adv. Funct. Mater.*, 2021, **31**, 2008146.
20. J. Chen, Z. Li, X. Wang, X. Sang, S. Zheng, S. Liu, B. Yang, Q. Zhang, L. Lei, L. Dai and Y. Hou, *Angew. Chem. Int. Ed.*, 2022, **61**, e202111683.
21. X. Hao, X. An, A. M. Patil, P. Wang, X. Ma, X. Du, X. Hao, A. Abudula and G. Guan, *ACS Appl. Mater.*, 2021, **13**, 3738-3747.

22. W. Ni, Z. Liu, Y. Zhang, C. Ma, H. Deng, S. Zhang and S. Wang, *Adv. Mater.*, 2021, **33**, e2003238.